Electronic Supplementary Material (ESI) for Journal of Materials Chemistry A.

Electronic Supplementary Information

Nacre-mimetic superstructure of poly(butylene succinate) structured by intense shear flow and ramie fiber as a promising strategy for simultaneous reinforcement and toughening

Xu-Long Xie,[a] Qiang-Sheng Sun,[a] Jun Lei,[a] Feng Tian,[b] Ling Xu,[a] Zheng Yan,[a] Gan-Ji Zhong *[a] and Zhong-Ming Li*[a]

[a] College of Polymer Science and Engineering, State Key Laboratory of Polymer Materials Engineering, Sichuan University, Chengdu, 610065, China

[b] Shanghai Institute of Applied Physics, Chinese Academy of Sciences, Shanghai, 201204, China

***Corresponding Authors:**

ganji.zhong@scu.edu.cn. (G.-J.Z.).

zmli@scu.edu.cn (Z.-M.L.)

1. Oscillation Shear injection Molding (OSIM)

The feature of a melt flow pattern in OSIM is quite different from that of conventional injection molding (CIM), and the crucial difference of two technologies exists in packing stage, whereas the other stages (i.e., preplasticizing, injection, etc.) are unchanged. The two pistons move out of phase during holding pressure, the shear force would make the PLA melt periodically move in the length direction of moldings, and the shear flow of PLA melt takes place until the gate is solidified. In other words, before being frozen, the PLA melt continuously undergoes oscillation shear stress, unless the pistons stop. As a result, the sufficiently high share rate (about 1000 s^{-1}) can impose on the melt in interior region with the increase of the thickness of solidified layer. Fig. S1 shows the digital photograph for OSIM apparatus[1], and Fig. S2 shows the local picture for the mold with an oscillation shear supplier[2]. The most difference is the part of mold with hot runner, which is illustrated in details in Fig. S3[3].

Fig. S1. Digital photograph showing the OSIM machine

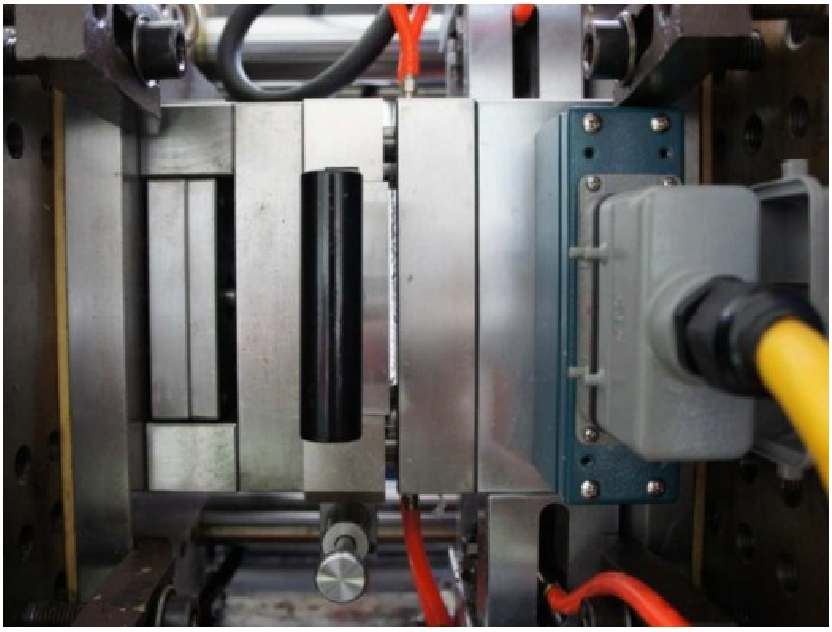

Fig. S2. Local picture for the mold with an oscillation shear supplier.

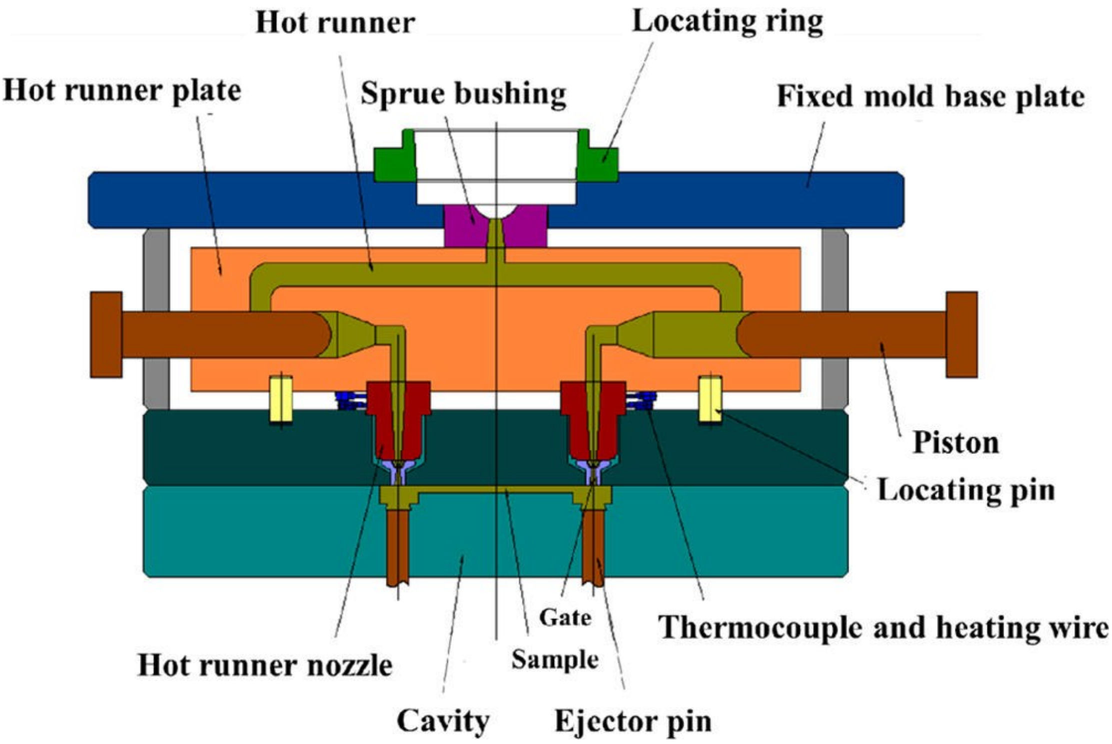

Fig. S3. Schematic illustration of OSIM mold with a hot runner part

2. Ramie fiber

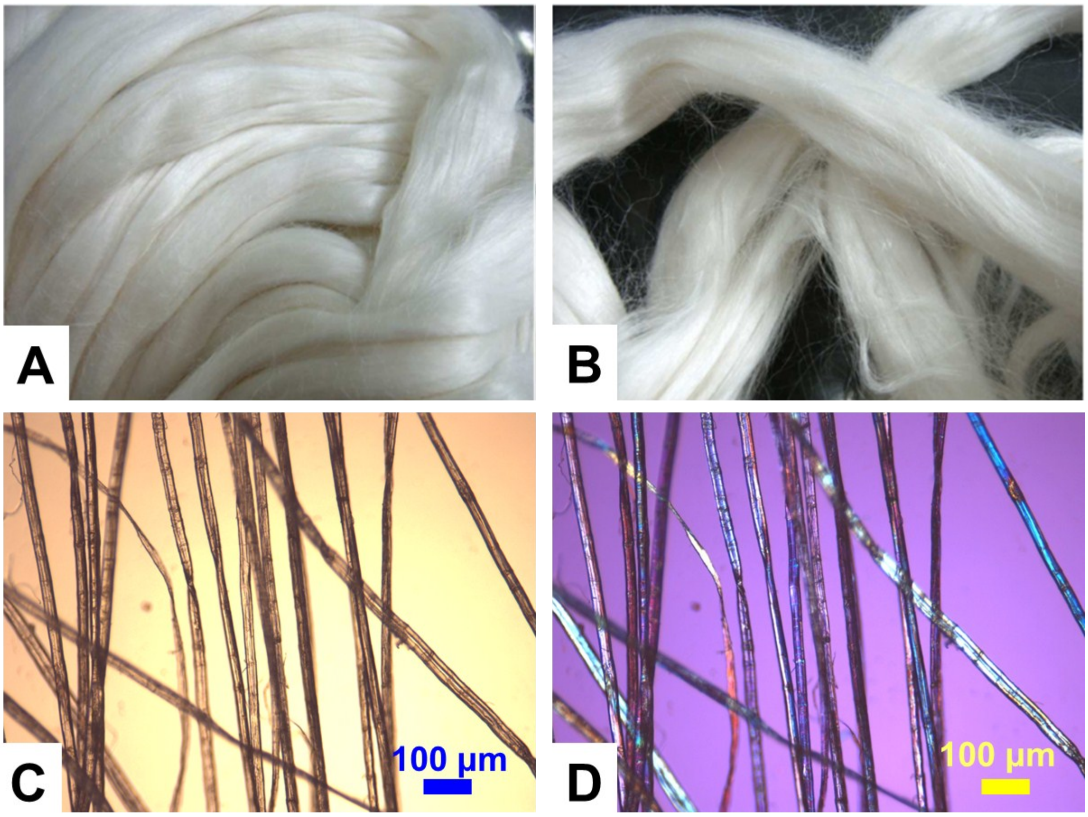

Fig. S4. Digital images (A) and (B), optical microscopic image (C) and polarized optical microscopic image (D) showing raw ramie fibers received from the manufacturer.

In our work, ramie fibers used are bast fibers from outer culm of ramie plant. Fig. S4(A) and (B) depict the overall appearance of our ramie fibers, showing separate bundles constituting a great quantity of bushy fibers with an average diameter of ~17 micrometer (Fig. S4(C) observed by optical microscopic image). From polarized optical microscopic image shown in Fig. S4(D), crystal exists in ramie fiber. As far as we are concerned, the ramie fibers are industrially fabricated during the pulping process using strong alkali solution for degumming, followed by repeating washing to remove the impurities.

3. The profile of shear rate and temperature in cavity during OSIM processing

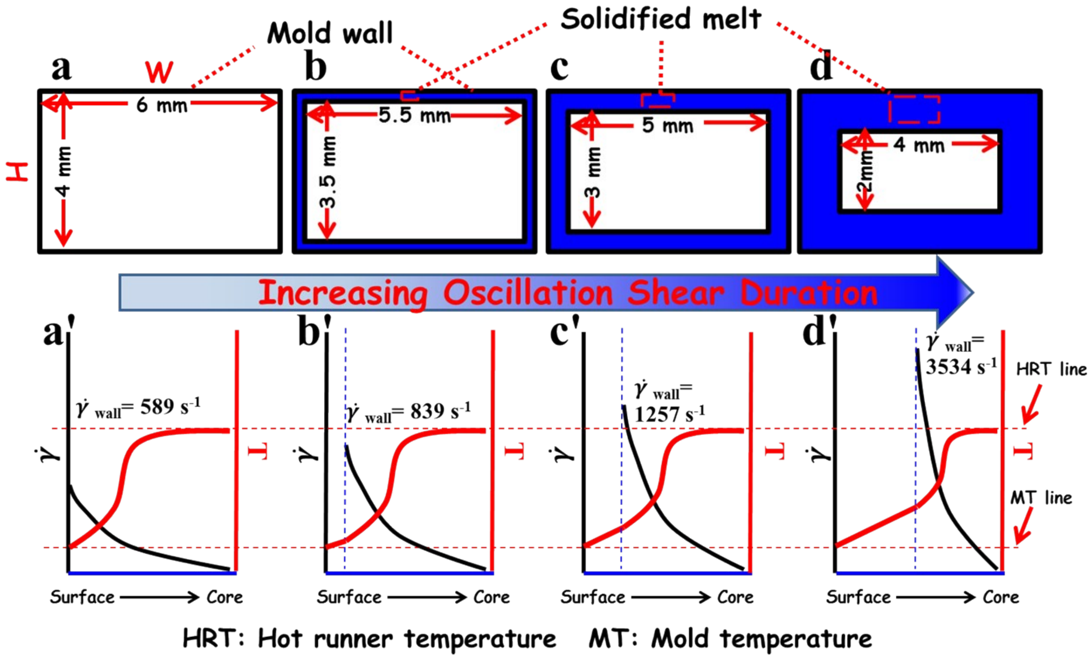

Fig. S5 Schematic depiction of (a-d) growth of solidified layer at a cross-section vertical to the flow direction, and (a′-d′) shear rate profile and temperature profile during solidification of melt in cavity. Oscillation shear duration increases from left to right.

Fig. S5 illustrates the profile of shear rate and temperature in cavity during OSIM processing, which is helpful for explanation of the results obtained. Fig.s S5 a-d show schematic depiction of the view at cross-section vertical to the flow direction during solidification in the mold cavity in the top row. Fig.s S5 a′-d′ in the bottom row show the profile of shear rate and temperature versus position from skin to core layers. Oscillation shear duration increases from left to right. With oscillation shear duration, the thickness of solidified layer increases because of a low mold temperature (40^{o}C). The shear rate near the walls can be calculated from Equation S1. The shear rate from skin to core is shown in bottom row with black line. Shortly after the start of flow, a flow profile develops with the maximum of shear rate near solidified line and zero at the center of the mold cavity (Fig. S5 a′-d′). Because the total volumetric flow rate remains constant, the maximum of shear rate experienced by the polymer melt at the solidified line increases. The red lines in the bottom row represent the temperature profile of polymer matrix from the solidified part to just solidified part then to the core part. The hot runner temperature in this work is 140 °C, so the temperature in the core layer of part is thought to be 140 °C. The temperature of solidified layer is near the mold temperature, and increases with the thickness of solidified layer, due to the poor heat transferring ability of polymer and the high temperature in the core layer. The temperature has a large impact on the relaxation of stretched chain. The stretched chains near the solidified layer can be inhibited from relaxation and remain to develop into aligned lamellae precursor. As a result, flow-induced aligned lamellae precursor near the wall leads to aligned lamellae with high density, and its density quickly falls off from the wall to the center of the mold cavity.

$$\dot{\gamma} = \frac{6q_v}{Wh^2}$$ • • • • • • • • • • • (**Equation S1**)

where q_v represents the volumetric flow rate (3π cm^3/s), W and h are the width and thickness of cross section of molten region, respectively.

4. The crystallinity and melting temperature of samples from the DSC heating curves

In this work, the lattice plane (110) of PBS overlap with the cellulose lattice plane crystal (200) of ramie fiber. It is difficult to calculate the accurate crystallinity of PBS by peak fitting. Therefore, the crystallinity of PBS was calculated by DSC in this work. DSC measurements were carried out using a TA DSC Q2000 instrument. Typically 4-5 mg samples were machined from the cross-section plane in the middle of the injection-molded bars. The samples were heated from 40 to 150 °C at a heating rate of 30 °C/min under nitrogen atmosphere. The crystallinity was calculated from the heating curve, according to the Equation S2, where ΔH_m is the measured melting enthalpy (from DSC) , X_{PBS} is the weight fraction of PBS, and ΔH_0 is the enthalpy of pure PBS crystal (200 J/g)[4].

$$X_c(\%) = \frac{\Delta H_m}{\Delta H_0 \times X_{PBS}} \times 100\%$$ • • • • • • • • • • • (**Equation S2**)

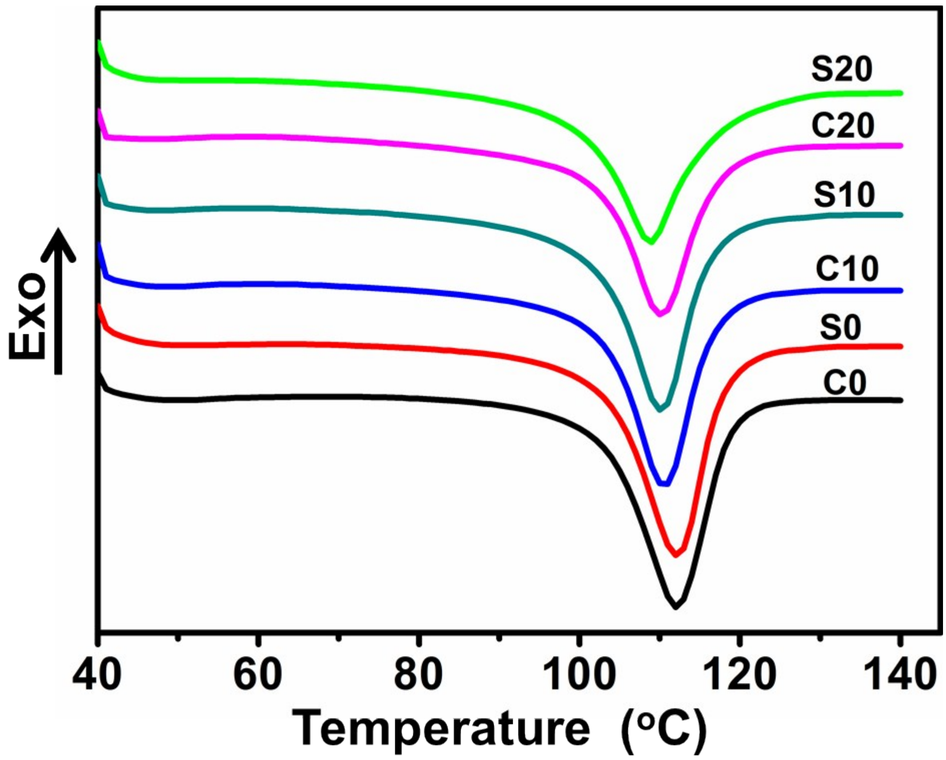

Fig. S6. DSC heating curves of structured and common PBS and PBS/Ramie Fiber biocomposites

For pure PBS and its composite samples, the heating curves are shown in Fig. S6. The heating curves have similar peaks, and the melting points of pure PBS and the composites are almost the same. As shown in Table S1, the crystallinity of common and structured PBS and its composites are quite similar, ranging from 36.1 to 38.8%. Therefore, the change of PBS crystallinity is so slight that it cannot induce an obvious impact on the mechanical properties.

Table S1. The crystallinity (X_c) of strcutured and common samples calculated from the DSC heating curves.

Samples	X_c (%)	
	C	S
PBS	36.1	37.3
10wt%RF	37.5	38.8

20wt%RF	37.5	37.1

5. The aligned and uniformly dispersed ramie fiber in PBS/ramie fiber composites parts

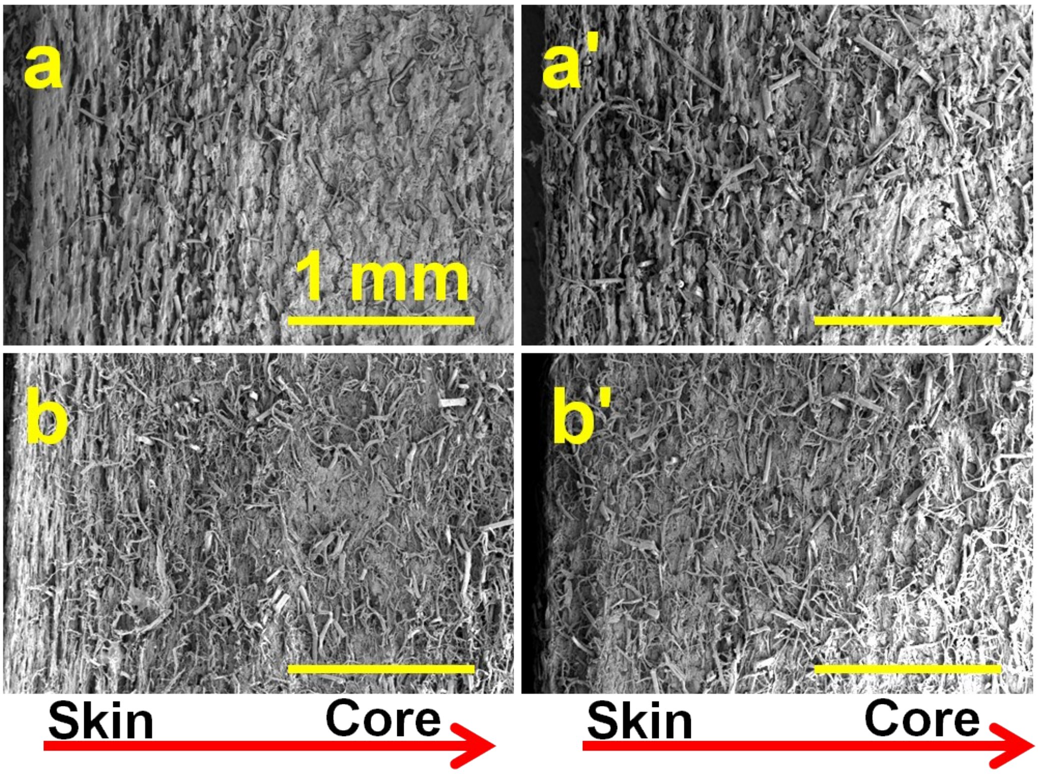

Fig. S7. SEM micrographs of etched PBS/ramie fiber composites with low magnification: (a and a') S10 and C10; (b and b') S20 and C20. The shear flow direction is vertical.

SEM was thus adopted to intuitively reveal the dispersion of ramie fiber in PBS matrix, as shown in Fig. S7. As a whole, the ramie fibers distribute uniformly in the optional region of parts, and show independence on the distance away from the skin layer, indicating good dispersion achieved by melting compounding (extrusion followed by injection molding). Intriguingly, the specific fiber alignment occurs not only in the skin layer, but also in the core layer.

6. The aligned crystalline lamellae at the skin layer of PBS and PBS/ramie fiber composites parts

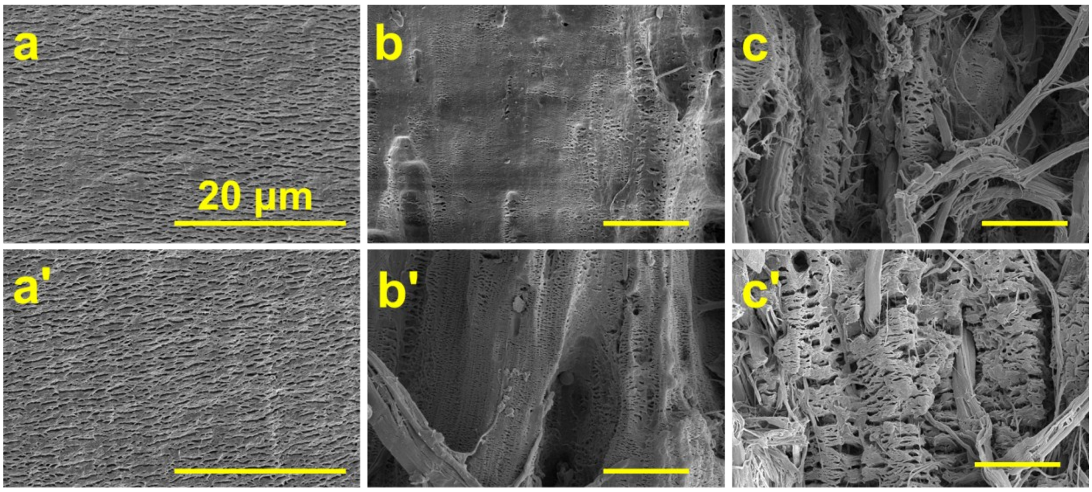

Fig. S8. SEM micrograph of etched injection molded PBS and PBS/ramie fiber biocomposites at the positions of 250 μm away from the surface. (a-c): S0, S10, S20; (a´-c´): C0, C10, C20. The shear flow direction is vertical.

We can see aligned lamellae at skin region (about 100μm away from the surface) of neat PBS and and PBS/ramie fiber biocomposites (shown in Fig. S8), because melts close to cool mold walls suffer high shear rate and cooling rate.

7. Crystalline structure and its distribution of structured PBS and PBS/ramie fiber composites by microbeam WAXD

A scanning microbeam two-dimensional WAXD measurement was carried out at BL15U of the Shanghai Synchrotron Radiation Facility (SSRF), China. The wavelength of the synchrotron radiation was 1.24 Å. A Mar165 CCD detector (2048 × 2048 pixels with pixel size of 80 μm) was employed to collect two-dimensional patterns. The distance between sample and detector was 160 mm. To characterize the crystalline structure from the skin to core layers, five positions: 100 and 500 (skin layer), 1000, 1500 (intermediate layer), 2000 μm (core layer) down from surface to inner, were scanned. The schematic diagram can be seen Fig. 2 in the article. 1D-WAXD profiles were obtained from circularly integrated intensities of 2D-WAXD image patterns. For evaluation of molecular orientation, a quantitative measurement was carried out using the Hermans′ orientation function defined as follows[5]:

$$f_H = \frac{3(<cos^2\varphi>-1)}{2} \quad \cdots\cdots\cdots\cdots \text{(Equation S3)}$$

Where $<cos^2\varphi>$ is the orientation factor defined as

$$<cos^2\varphi> = \frac{\int_0^{\pi/2} I(\varphi)\, cos^2\varphi\, sin\varphi d\varphi}{\int_0^{\pi/2} I(\varphi)\, sin\varphi d\varphi} \quad \cdots\cdots\cdots\cdots \text{(Equation S4)}$$

where φ is the angle between the normal of a given (*hkl*) crystal plane and shear flow direction, and $I(\varphi)$ is the intensity. The orientation function $f_H = 1$ when the probed axis is perfectly parallel to the reference direction, $f_H = -0.5$ when the probed axis is perfectly perpendicular to the reference direction, and $f_H = 0$ when the probed axis is randomly distributed. The orientation parameter of nacre-mimetic and common samples was calculated mathematically using Picken's method from q=14.1 nm^{-1} (i.e., 020 reflections) of WAXD.

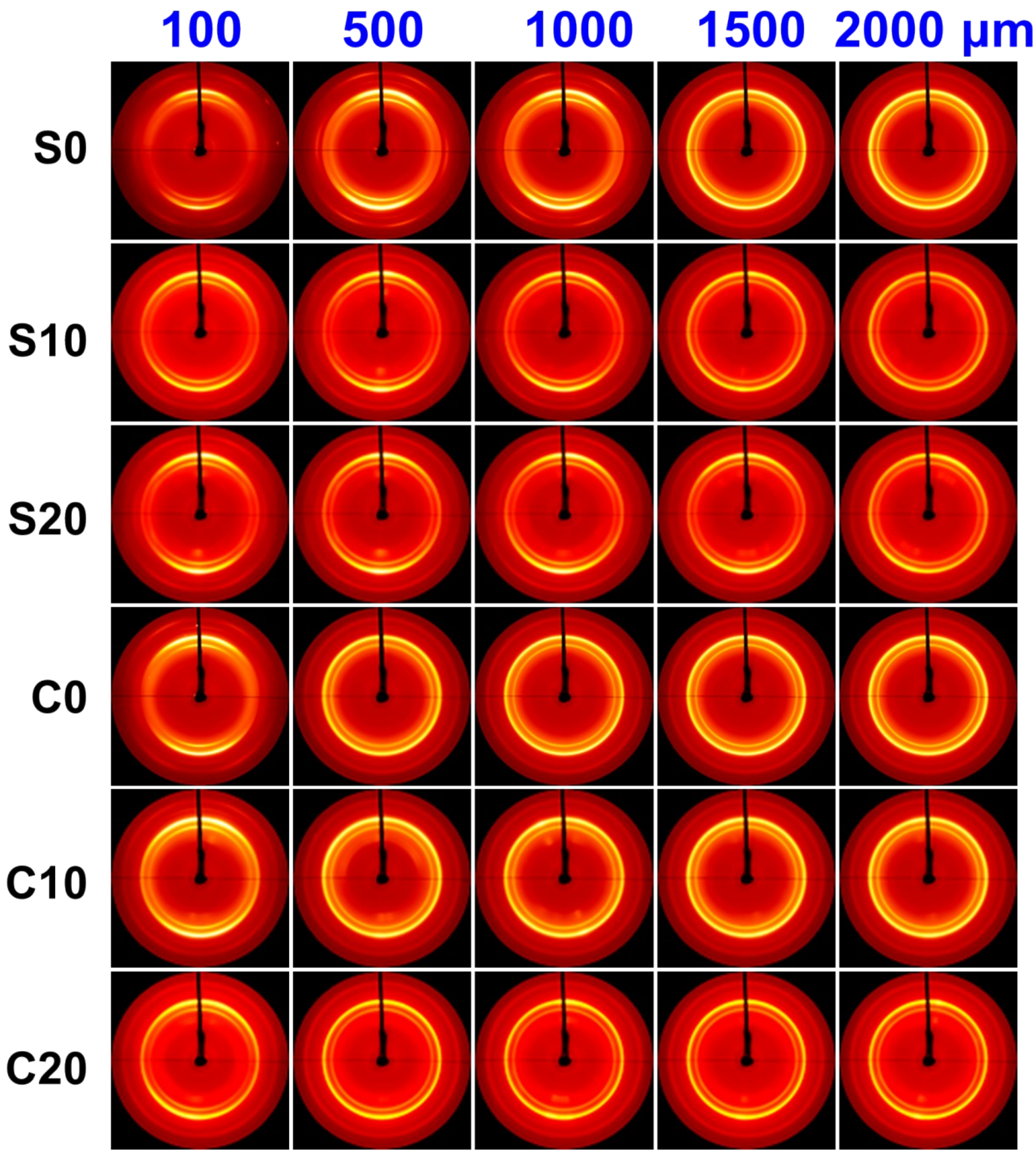

Fig. S9. 2D-WAXD patterns of structured and common samples at different regions away from the surface. The shear flow direction is horizontal.

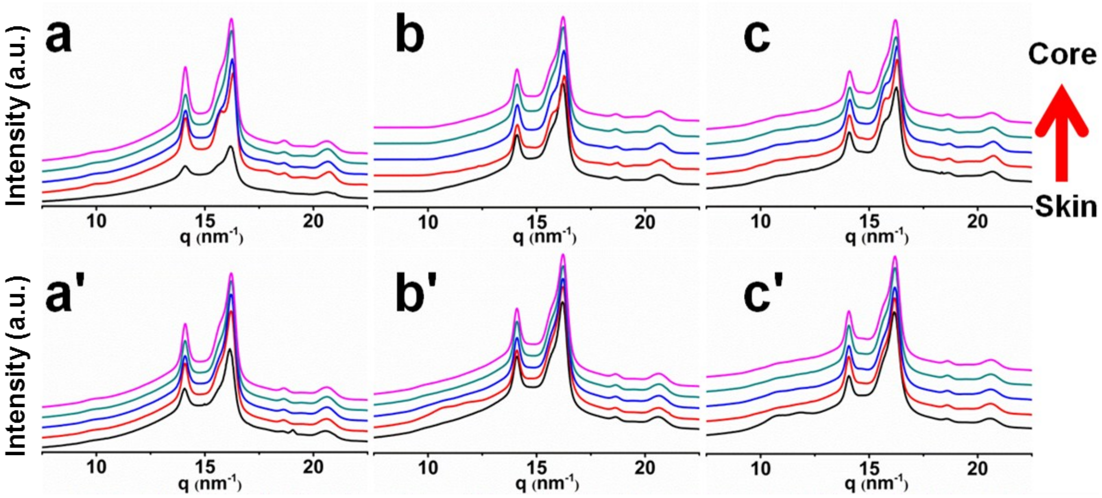

Fig. S10. WAXD curves from 2D-WAXD patterns of structured and common neat PBS and PBS/ramie fiber composites at different regions away from the surface. (a-c): S0, S10, S20; (a´-c´): C0, C10, C20.

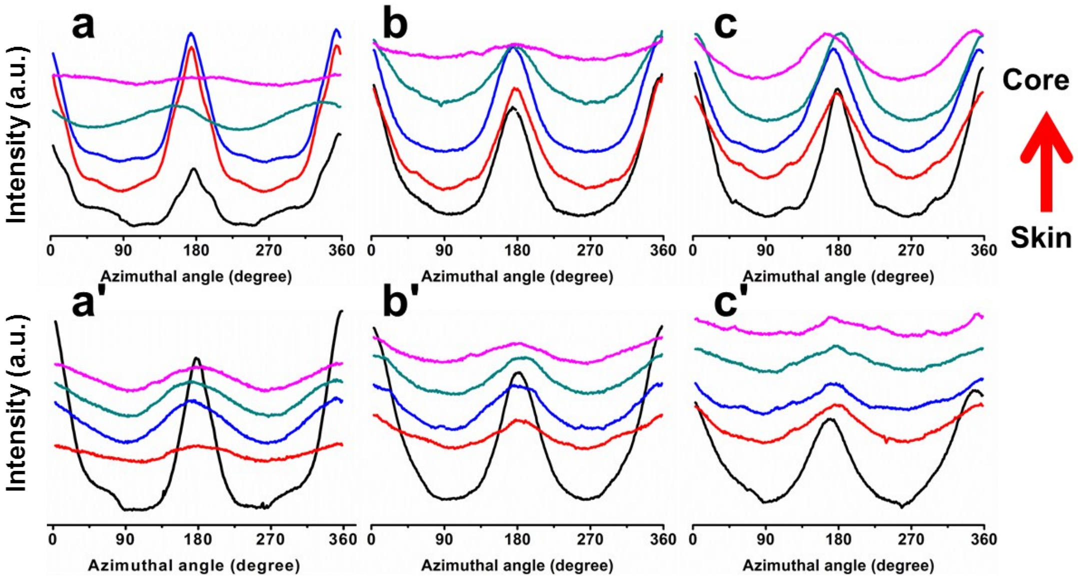

Fig. S11. Intensity distribution of the (020) plane along azimuthal angle of α crystal of structured and common neat PBS and PBS/ramie fiber composites at different regions away from the surface. (a-c): S0, S10, S20; (a´-c´): C0, C10, C20.

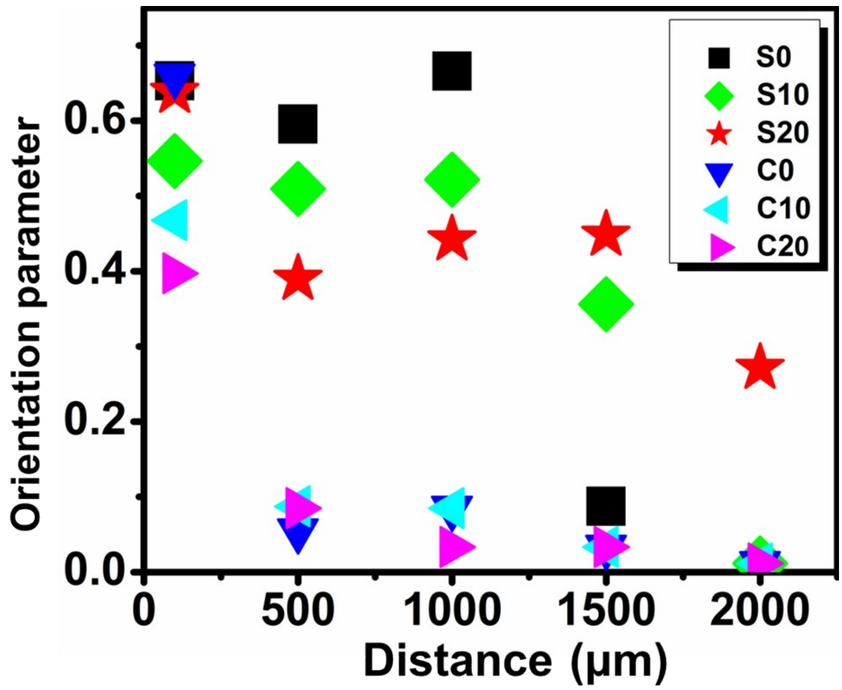

Fig. S12. Orientation parameter of structured and common neat PBS and PBS/ramie fiber composites calculated from the azimuth diffraction curves of the (020) plane.

The specific structural information on crystalline superstructure in structured and common PBS and PBS/ramie fiber composites from skin to core layer is revealed by utilizing the microbeam WAXD. Fig. S9 shows the 2D-WAXD patterns of S0, S10, S20, C0, C10 and C20 from different layers, viz. skin (location of 100 and 500 μm away from surface), intermediate (locations of 1000 and 1500 μm away from surface) and core (location of 2000 μm away from surface) layers. WAXD intensity profiles are integrated circularly from the corresponding 2D-WAXD patterns as shown in Fig. S10. Three main characteristic diffraction peaks located at q=14.1, 15.8, 16.3 nm^{-1} are assigned to (020), (021) and (110) planes of α-form PBS crystal, respectively.[4] The structured and common samples have the similar peaks at the same location, indicating that they have the same crystal structure (α-form crystal of PBS even if the crystallization condition may be different. Importantly, the arclike diffractions in Fig. S8 demonstrate the chain segment orientation in lamellae, while isotropic diffraction circles indicate no appreciable oriented structure. In order to reveal the orientation degree of the molecular chains, the (020) intensity distribution along the azimuthal angle between 0 and 360° was integrated and shown in Fig. S11. The orientation of lamellae can be directly reflected by the azimuthal width[6]. Meanwhile, the orientation parameters are also estimated from the intensity of the (020) along azimuthal angle and shown in Fig. S12. From WAXD results, it can be ensured that abundant aligned crystalline lamellae were formed in S0, S10 and S20 and randomly organized crystalline lamellae were formed in almost regions of C0, C10 and C20. The presence of ramie fiber helps us fabricate more nacre-mimetic superstructure under intense shear flow.

References

1. H. Xu, L. Xie, Y. -H. Chen, H. -D. Huang, J. -Z. Xu, G. -J. Zhong, B. S. Hsiao, Z. -M. Li, *ACS Sustain. Chem. Eng.,*2013**, 1**, 1619-1629.

2. H. Xu, G. -J. Zhong, Q. Fu, J. Lei, W. Jiang, B. S. Hsiao, Z. -M. Li, *ACS Appl. Mater. Interfaces,* 2012**, 4**, 6773-6783.

3. Z. Zhang, R. Zhang, Y. Huang, J. Lei, Y. -H. Chen, J. -H. Tang, Z. -M. Li, *Ind. Eng. Chem. Res.,* 2014, **53**, 10144-10154.

4. G. Liu, L. Zheng, X. Zhang, C. Li, S. Jiang, D. Wang, *Macromolecules,* 2012**, 45**, 5487-5493.

5. G. -J. Zhong, L. Li, E. Mendes, D. Byelov, Q. Fu, Z.-M. Li, *Macromolecules,* 2006**, 39**, 6771-6775.

6. H. -R. Yang, J. Lei, L. Li, Q. Fu, Z. -M. Li, *Macromolecules,* 2012**, 45**, 6600-6610.